Electronic Supplementary Material (ESI) for Journal of Materials Chemistry A.

The N, P co-doped carbon-loading Ni_3P@Ni heterojunction nanocomposites derived from polybenzimidazoles grafted with oxygen-phosphorus group as high-efficiency electrocatalyst for oxygen evolution reaction

Gang Wang[1]*, Wenshuai Tang[1], Shuai Yang[1], Mingxia Lu[1], Hongliang Wei[1], Lifeng Cui[2]* and Xiaodong Chen[3]*

[1] College of Chemistry and Chemical Engineering, Henan University of Technology, Zhengzhou 450001, PR China

[2] College of Smart Energy, Shanghai Jiao Tong University, Shanghai 200240, PR China

[3] *Department of Mechanical Engineering, City University of Hong Kong, Tat Chee Avenue, Kowloon, Hong Kong SAR, China.*

Figure captions

Figure S1. The synthetic route of PBI-OP.

Figure S2. TG curves of Ni/PBI-OP precursor.

Figure S3. The pore size distribution curves of PBI-OP, Ni_3P@Ni/CNP-L, Ni_3P@Ni/CNP-M and Ni_3P@Ni/CNP-H.

Figure S4. Magnified SEM images of Ni/PBI-OP.

Figure S5. (a) TEM image and (b) HRTEM images of PBI-OP.

Figure S6. (a) TEM image and (b) HRTEM images of Ni/PBI-OP Precursor.

Figure S7. Magnified SEM images of (a) Ni_3P@Ni/CNP-L and (b) Ni_3P@Ni/CNP-H.

Figure S8. AFM image of (a) Ni_3P@Ni/CNP-L, (b) Ni_3P@Ni/CNP-M, (c) Ni_3P@Ni/CNP-H, and height contour at the red dashed line of (d) Ni_3P@Ni/CNP-L, (e)Ni_3P@Ni/CNP-M and (f) Ni_3P@Ni/CNP-H.

Figure S9. (a) TEM image, (b) HRTEM images of Ni_3P@Ni/CNP-L.

Figure S10. (a) TEM image, (b) HRTEM images of Ni_3P@Ni/CNP-H.

Figure S11. (a) XPS survey, (b) C1s, (c) N1s, (d) Ni2p, (e) O1s, and (f) P2p spectrums of Ni_3P@Ni/CNP-L.

Figure S12. (a) XPS survey, (b) C1s, (c) N1s, (d) Ni2p, (e) O1s, and (f) P2p spectrums of Ni_3P@Ni/CNP-H.

Figure S13. The XPS (a) C1s, (b) N1s, (c) O1s and (d) P2p spectrum of PBI-OP.

Figure S14. In real electrolytic cell Ni_3P@Ni /CNP electrocatalyst.

Figure S15. CV curves of (a) PBI-OP, (b) Ni_3P@Ni/CNP-L, (c) Ni_3P@Ni/CNP-M and (d) Ni_3P@Ni/CNP-H.

Figure S16. XRD pattern of Ni_3P@Ni/CNP-M after 48h test.

Figure S17. TEM of Ni_3P@Ni/CNP-M after 48h test.

Figure S18. (a) XPS survey, (b) Ni2p, (c) C1s, (d) N1s, (e) O1s, and (f) P2p spectrums of Ni_3P@Ni/CNP-M after 48h test.

Figure S19. CV curves in 1M KOH before and after addition of 1 M CH_3OH of (a) PBI-OP, (b) Ni_3P@Ni/CNP-L and (c) Ni_3P@Ni/CNP-H.

Figure S20.The optimized structure of Ni_3P@Ni, side view(left); top view(right). (Lattice parameters a = 9.44 Å, b = 12.66 Å, c = 27.30 Å, $\alpha = 90°$, $\beta = 90°$, $\gamma = 90°$).

Figure S21. The optimized structure of IrO_2, side view(left); top view(right). (Lattice parameters a = 9.56 Å, b = 12.82 Å, c = 23.87 Å, α = 90°, β= 90°, γ= 90°).

Table captions

Table S1. The surface area, total pore volume and pore size of PBI-OP，Ni_3P@Ni/CNP-L, Ni_3P@Ni/CNP-M, and Ni_3P@Ni/CNP-H.

Table S2 Elemental and ICP-OES analyses of Ni_3P@Ni/CNP sample.

Table S3. The XPS peak separation ratio of N1s for Ni_3P@Ni/CNP-L, Ni_3P@Ni/CNP-M, and Ni_3P@Ni/CNP-H.

Table S4. Comparison of electrocatalytic OER activities of Ni_3P@Ni/CNP-M with similar state-of-the-art OER electrocatalysts.

Table S5 Elemental and ICP-OES analyses of Ni_3P@Ni/CNP-M before and after 48h test.

Table S6. EIS fitting parameters to the equivalent electric circuit for the OER.

DFT calculation: Density generalized function theory (DFT) calculations were performed using the firstness principle [1]-[2] in the generalized gradient approximation (GGA) using the Perdew-Burke-Ernzerhof (PBE) formulation [3]. We choose the projected augmented wave (PAW) potential [4][5] to describe the ionic nuclei, while the plane wave base set with a kinetic energy cutoff of 450 eV was used to consider the valence electrons. Van der Waals interactions were considered using grime's DFT-D3 method [6][7]. When the energy change was less than 10^{-5} eV, the electron energy was considered self-consistent. The geometric optimization was considered convergent when the energy change was less than 0.02 eV $Å^{-1}$. The Brillouin region integration was performed in Gamma k point grid 0.04 $Å^{-1}$ to optimize the lattice size and geometry. To eliminate artificial effects between periodic images, A 15 Å vacuum layer was added to the surface. The spin polarization was calculated.

Using the computational hydrogen electrode (CHE) model developed by Nørskov et al. [8], we established an adsorption model to calculate the Gibbs free energy of oxygen evolution reaction (OER). The reaction mechanism of OER was as follows [9][10]:

$$* + OH^- \rightarrow *OH + e^-$$

$$*OH + OH^- \rightarrow *O + H_2O_{(l)} + e^-$$

$$*O + OH^- \rightarrow *OOH + e^-/*O+*OH++ e^-$$

$$*OOH + OH^- \rightarrow * + O_{2(g)} + H_2O_{(l)} + e^-/*O+*OH + OH^-\rightarrow *O+*O+ H_2O_{(l)} + e^-$$

$$*O+*O \rightarrow O_{2(g)}$$

where * indicated the bare surface. The free energy change was defined as follow: $\Delta G = \Delta E + \Delta E_{zpe} - T\Delta S + \Delta G_{pH} - eU$, where ΔE, ΔE_{ZPE} and ΔS represented the difference of total energy, zero-point energy, and entropy between products and reactants for all elementary reactions. The value of ΔG_{pH} was 0.828 eV at pH=14 according to $\Delta GpH = -kBTln[H^+]$. U and e were the electrode potential and transferred charge, respectively. The entropies of the free molecule H_2O were referenced to the NIST database[10]. Meanwhile, we obtained the free energy of O_2 by the equation of $G(O_2) = 4.92 + 2G(H_2O) - 2(H_2)$, due to the bad description of magnetism of O_2 in VASP.

References

[1] G. Kresse, J. Furthmüller, Efficiency of ab-Initio total energy calculations for metals and semiconductors ssing a plane-wave basis, Set. Comput. Mater. Sci. 6 (1996) 15−50.

[2] G. Kresse, J. Furthmüller, Efficient iterative schemes for Ab initio total-energy calculations using a plane-wave basis, Set. Phys. Rev. B 54 (1996) 11169−11186.

[3] J.P. Perdew, K. Burke, M. Ernzerhof, Generalized gradient approximation made, Simple. Phys. Rev. Lett. 77 (1996) 3865−3868.

[4] G. Kresse, D. Joubert, From ultrasoft pseudopotentials to the projector augmented-wave method, Phys. Rev. B 59 (1999) 1758-1775.

[5] P.E. Blöchl, Projector augmented-wave method, Phys. Rev. B 50 (1994) 17953-17979.

[6] S. Grimme, J. Antony, S. Ehrlich, H. Krieg, A consistent and accurate ab initio parametrization of density functional dispersion correction (DFT-D) for the 94 elements H-Pu, J. Chem. Phys. 132, (2010) 154104.

[7] S. Grimme, S. Ehrlich, L. Goerigk, Effect of the damping function in dispersion corrected density functional theory, J. Comput. Chem., 2011, 32, 1456-1465.

[8] E. Skúlason, G.S. Karlberg, J. Rossmeisl, T. Bligaard, J. Greeley, H. Jónsson, J.K. Nørskov, Density functional theory calculations for the hydrogen evolution reaction in an electrochemical double layer on the Pt(111) electrode, Phys. Chem. Chem. Phys. 9 (2007) 3241-3250.

[9] M. Plevová, J. Hnát, K. Bouzek, Electrocatalysts for the oxygen evolution reaction in alkaline and neutral media. A comparative review, J. Power Sources 2021, 230072.

[10] C. Hu, L. Zhang, J. Gong, Recent progress made in the mechanism comprehension and design of electrocatalysts for alkaline water splitting, Energy Environ. Sci. 12 (2019) 2620-2645.

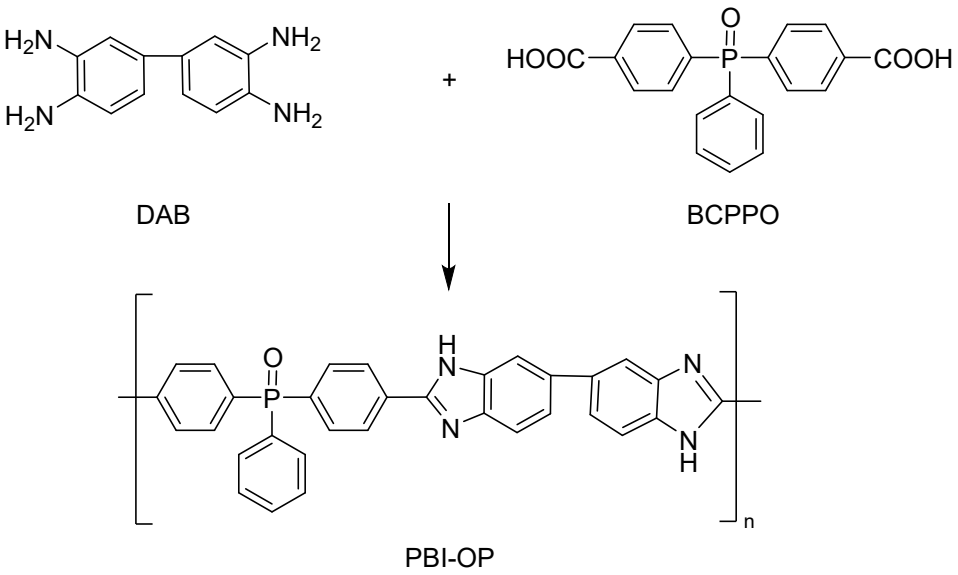

Figure S1. The synthetic route of PBI-OP.

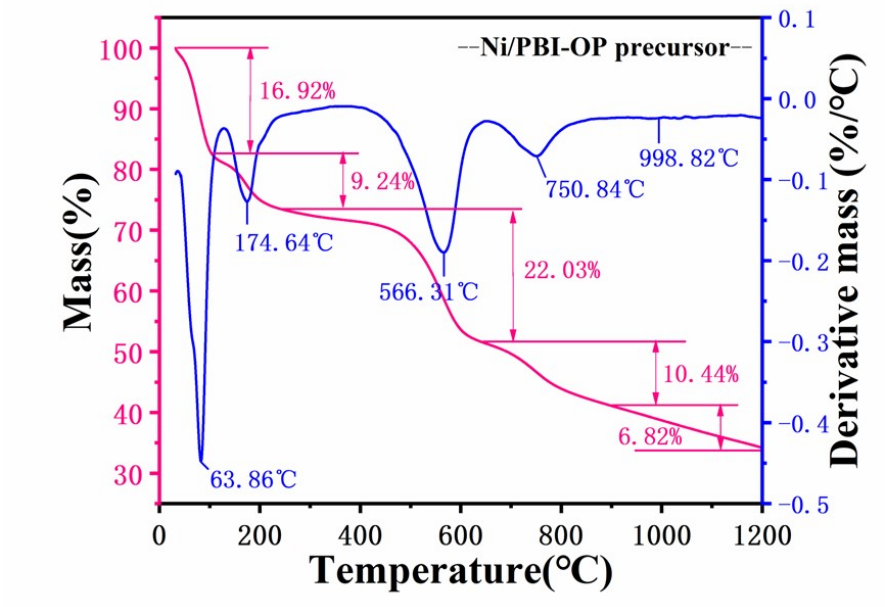

Figure S2. TG curves of Ni/PBI-OP precursor.

The TG/DTA curves of Ni/PBI-OP precursor in N_2 atmosphere were exhibited in Figure S2. The whole weight loss process could be divided into five processes. The weight loss of 16.92% at 63.86°C was due to the removal of free water from the sample, and the second weight loss occurred at 174.64°C due to the loss of bound water in the sample ($NiCl_2 \cdot 6H_2O \rightarrow NiCl_2 + 6H_2O$) with a loss of 9.24% by weight[1]. A third weight loss was recorded at 566.31℃ because the main chain of the PBI-OP polymer was broken down at high temperature [2-4], both Ni and Ni_3P are generated, and a total of 22.03% of weight was lost in this stage. The fourth weight loss was 10.44%, which occurs at 750.84℃. The reason was that Ni_3P will decompose into Ni with the increase of temperature[5], and CNP material would also be further decomposed. The last weight loss (6.82%) was recorded at 998.82℃, which was due to the oxidation of low-valence Ni_3P to high- valence Ni_5P_4 at high temperature[6].

Reference

[1] J.N. Charles, N.D. Deshpande, D.A. Deshpande, Dehydration of $NiCl_2 \cdot 6H_2O$, THERMOCHIMICA ACTA (2001).

[2] G. Wang, G. Xiao, D. Yan, Synthesis and properties of soluble sulfonated polybenzimidazoles derived from asymmetric dicarboxylic acid monomers with

sulfonate group as proton exchange membrane, Journal of Materials Science 369(1-2) (2011) 388-396.

[3] G. Wang, S. Yang, M. Lu, B. Hua, Z. Zhang, J. Kang, W. Tang, H. Wei, L. Cui, X. Chen, Sulfonated polybenzimidazole engineering defect-induced N, S-codoped carbon-supported Co3C hybrid composite as high-efficiency electrocatalyst for oxygen evolution reaction, Electrochimica Acta 443 (2023) 141939.

[4] G. Wang, Y. Yao, G. Xiao, D. Yan, Novel sulfonated polybenzothiazoles with outstanding dimensional stability for proton exchange membranes, Journal of Membrane Science 425-426 (2013) 200-207.

[5] G. Shi, J. Shen, New synthesis method for nickel phosphide nanoparticles: solid phase reaction of nickel cations with hypophosphites, Journal of Materials Chemistry 19(16) (2009) 2295-2297.

[6] Q. Guan, W. Li, M. Zhang, K. Tao, Alternative synthesis of bulk and supported nickel phosphide from the thermal decomposition of hypophosphites, Journal of Catalysis 263(1) (2009) 1-3.

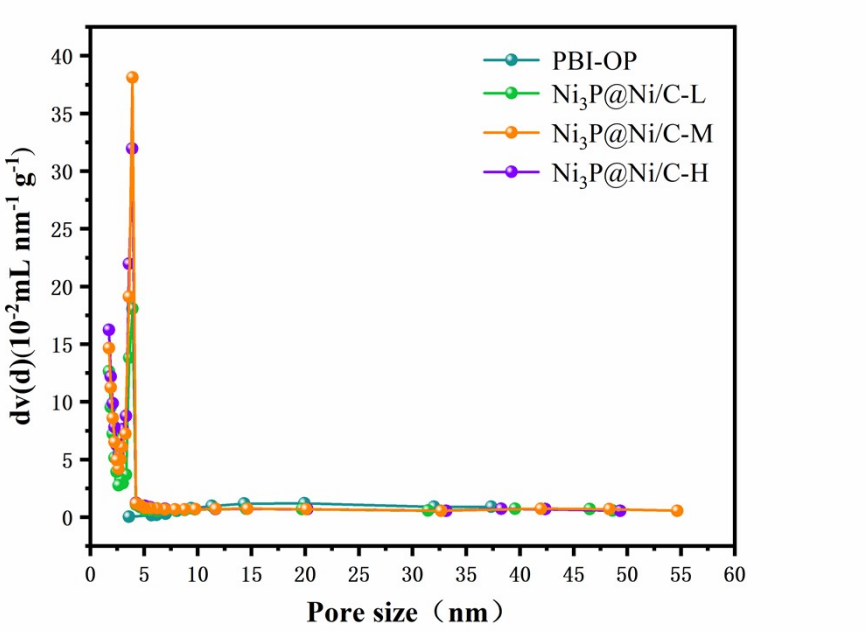

Figure S3. The pore size distribution curves of PBI-OP and Ni_3P@Ni/CNP-L, Ni_3P@Ni/CNP-M, and Ni_3P@Ni/CNP-H.

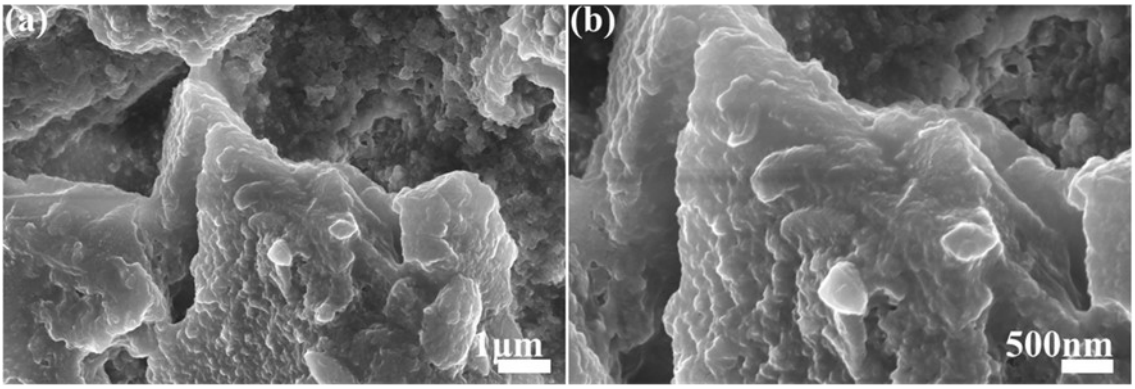

Figure S4. Magnified SEM images of Ni/PBI-OP.

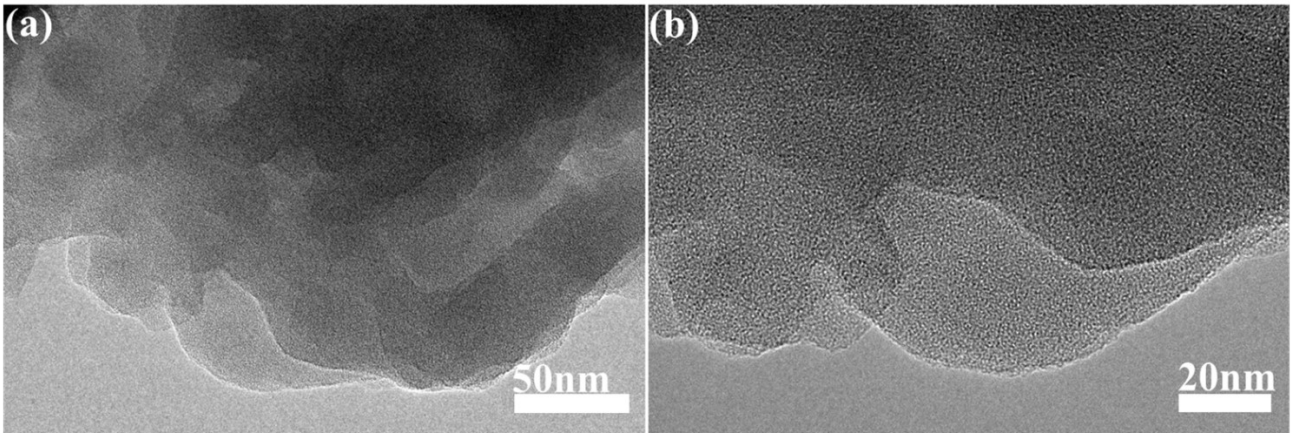

Figure S5. (a) TEM image and (b) HRTEM images of PBI-OP.

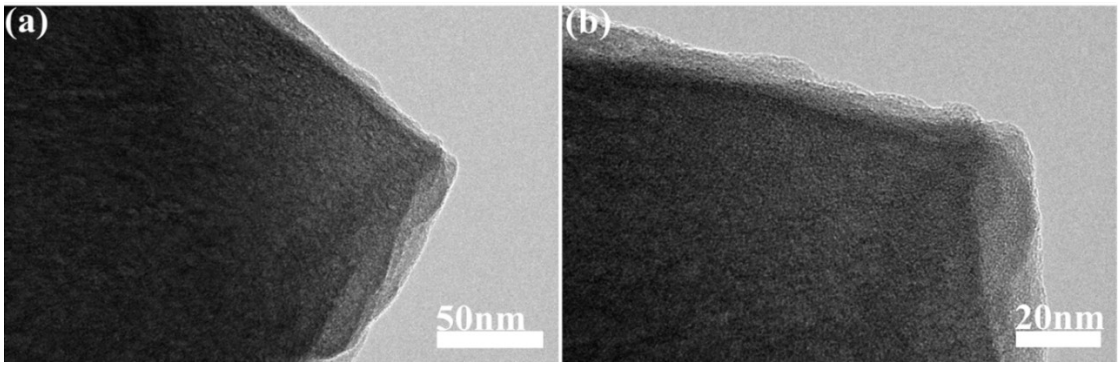

Figure S6. (a) TEM image and (b) HRTEM images of Ni/PBI-OP Precursor.

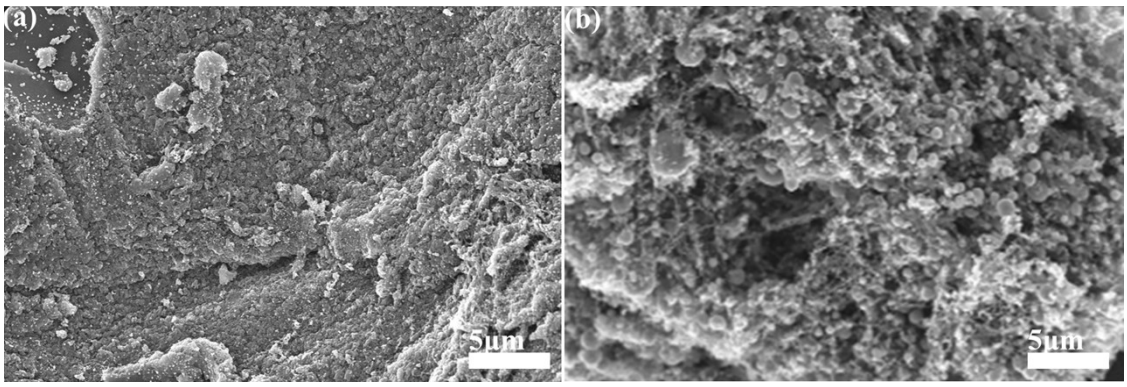

Figure S7. Magnified SEM images of (a) Ni_3P@Ni/CNP-L and (b) Ni_3P@Ni/CNP-H.

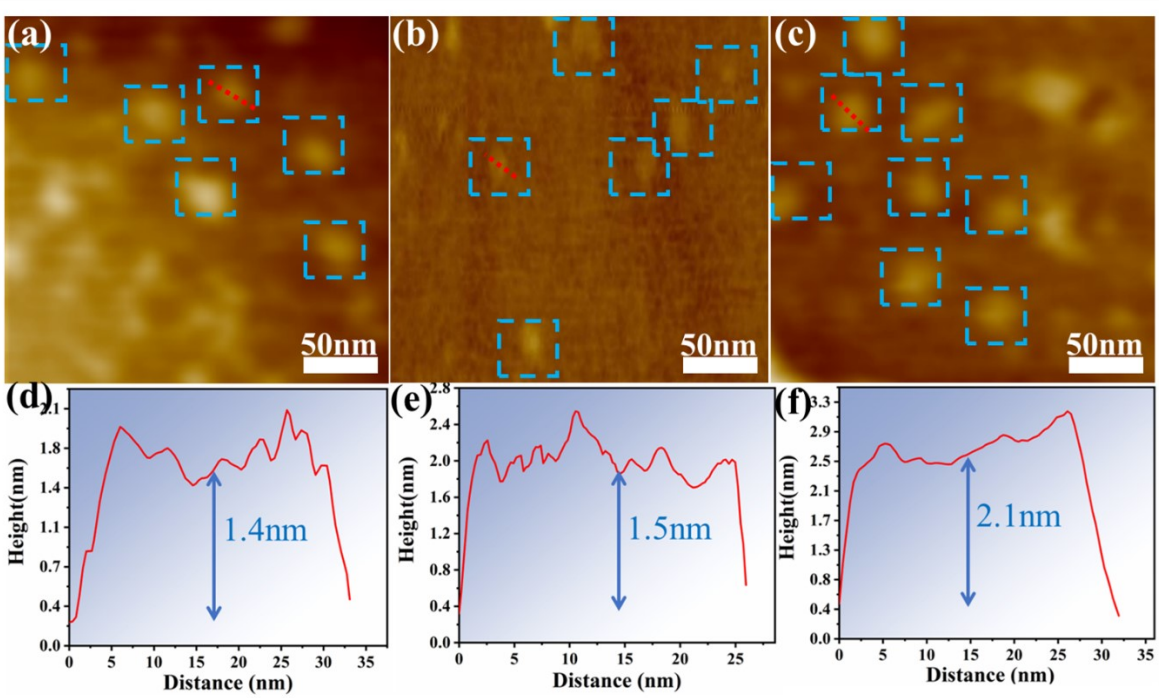

Figure S8. AFM image of (a) Ni_3P@Ni/CNP-L, (b) Ni_3P@Ni/CNP-M, (c) Ni_3P@Ni/CNP-H, and Height contour at the red dashed line of (d) Ni_3P@Ni/CNP-L, (e) Ni_3P@Ni/CNP-M, (f) Ni_3P@Ni/CNP-H.

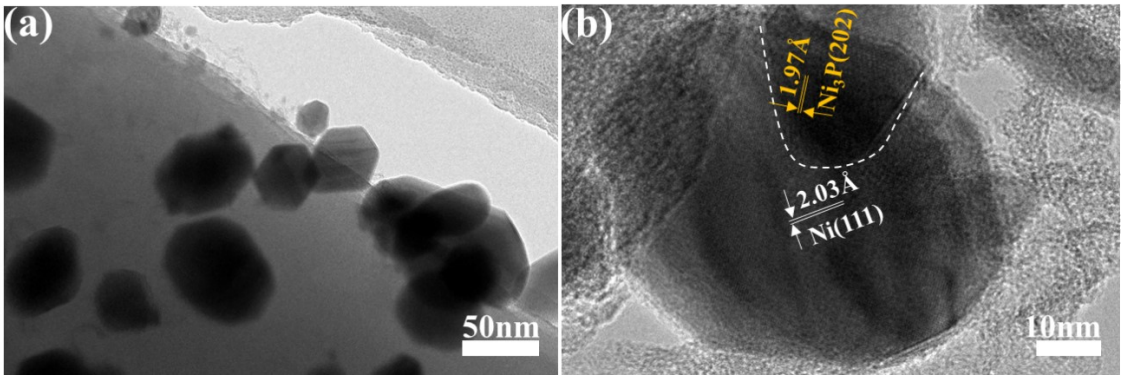

Figure S9. (a) TEM image, (b) HRTEM images of Ni_3P@Ni/CNP-L.

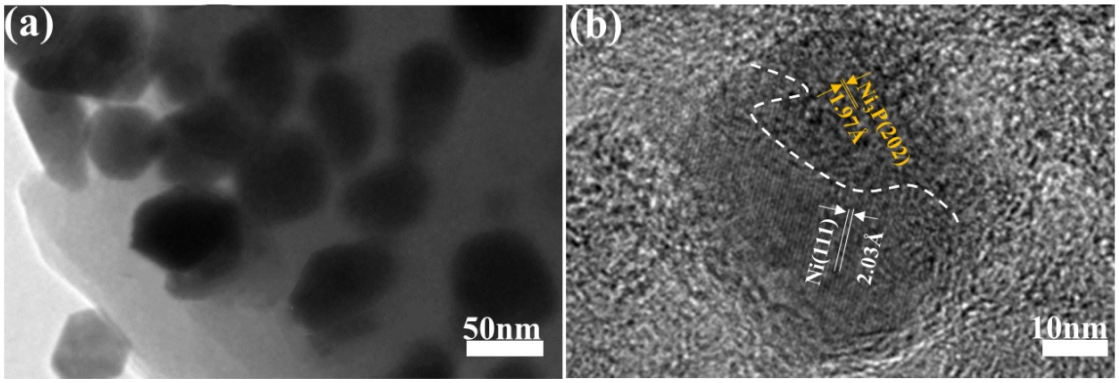

Figure S10. (a) TEM image, (b) HRTEM images of Ni_3P@Ni/CNP-H.

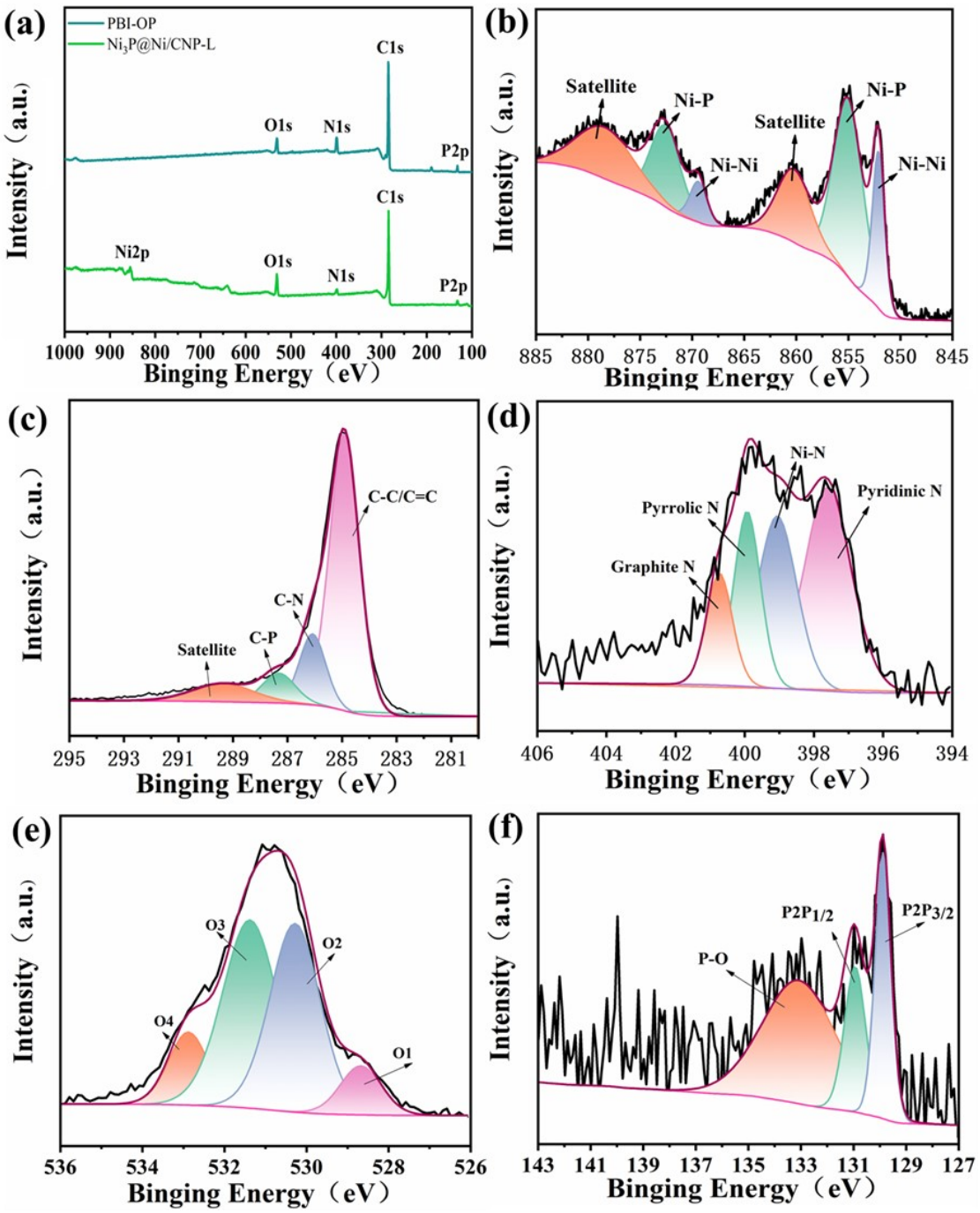

Figure S11 (a) XPS survey, (b) Ni2p, (c) C1s, (d) N1s, (e) O1s, and (f) P2p spectrums of Ni_3P@Ni/CNP-L.

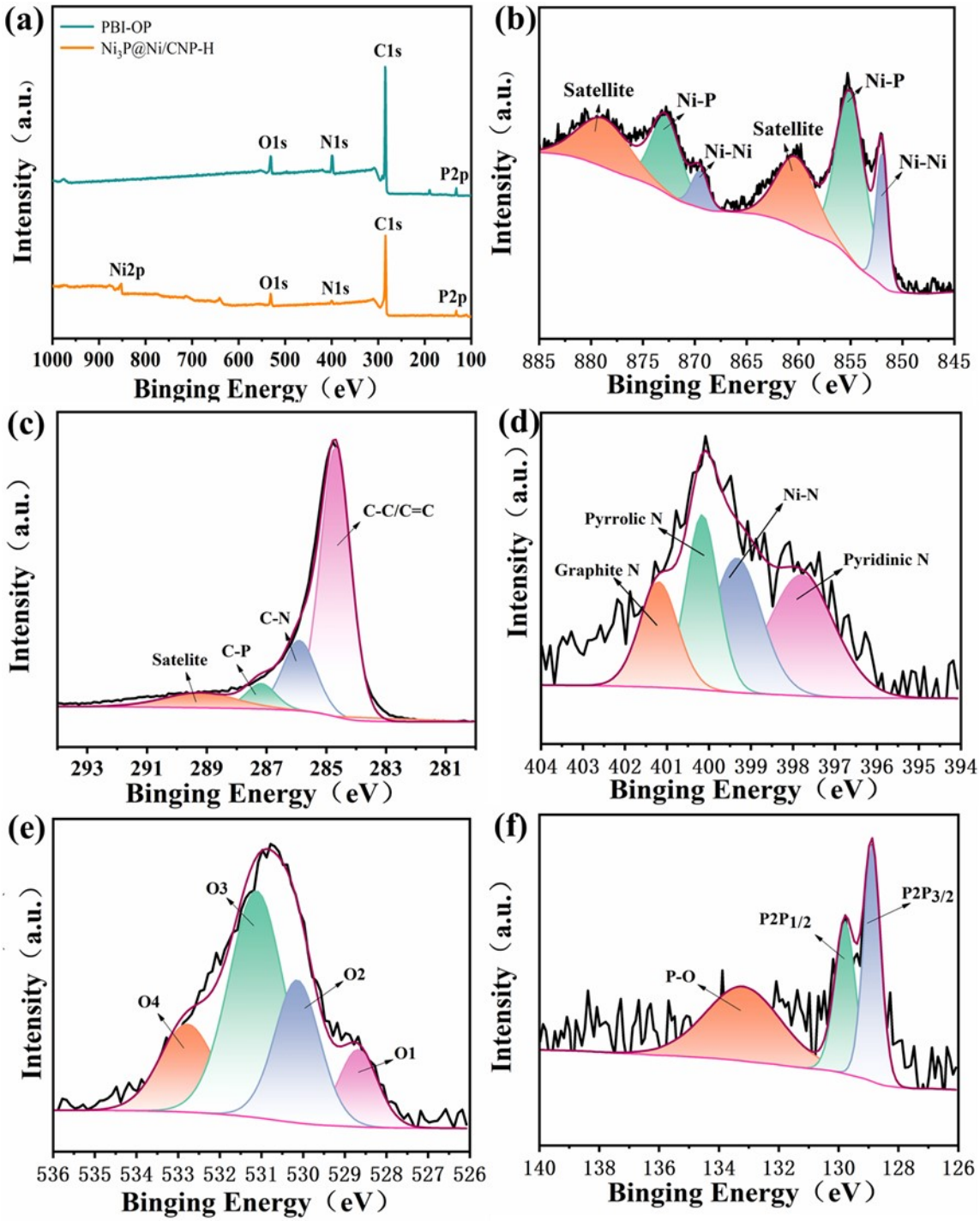

Figure S12. (a) XPS survey, (b) Ni2p, (c) C1s, (d) N1s, (e) O1s, and (f) P2p spectrums of Ni_3P@Ni/CNP-H.

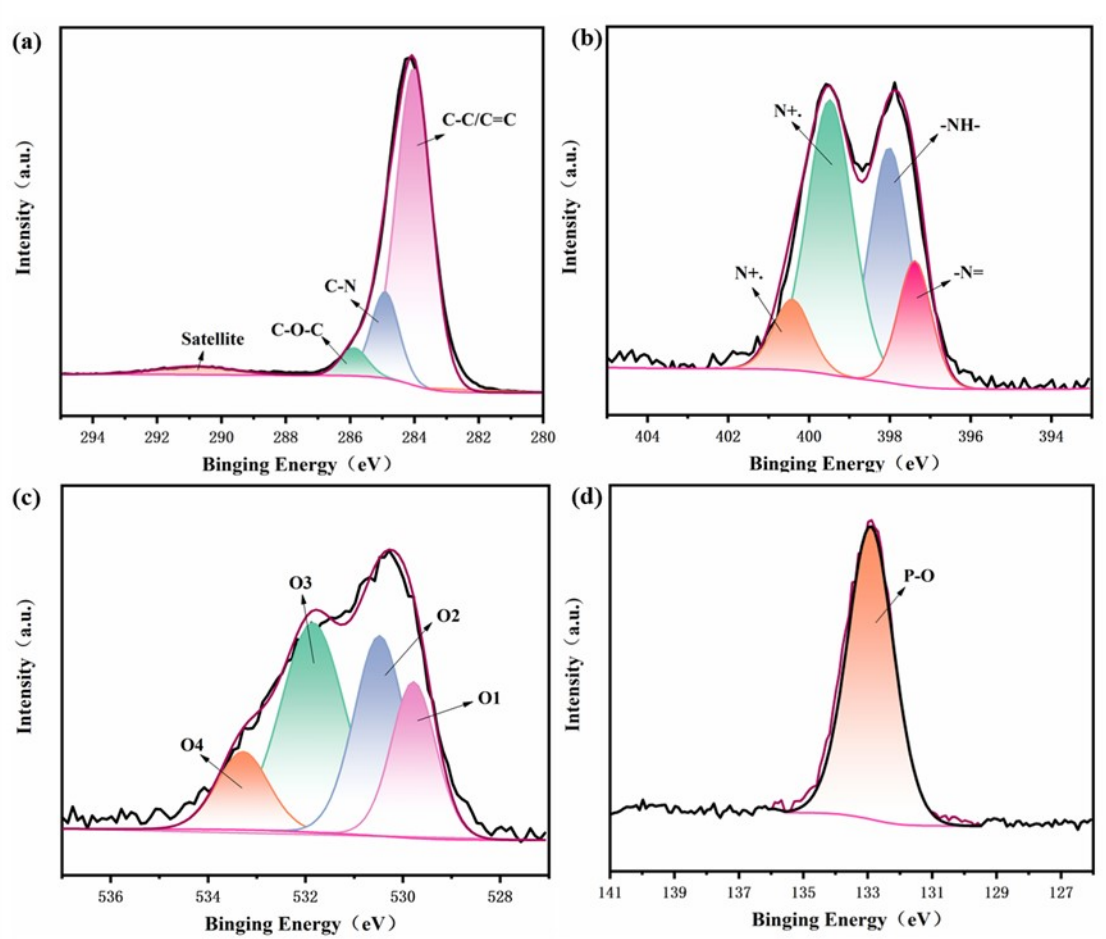

Figure S13. The XPS (a) C1s, (b)N1s, (c) O1s and (d) P2p spectrum of PBI-OP.

Figure S14. In real electrolytic cell Ni_3P@Ni/CNP electrocatalyst.

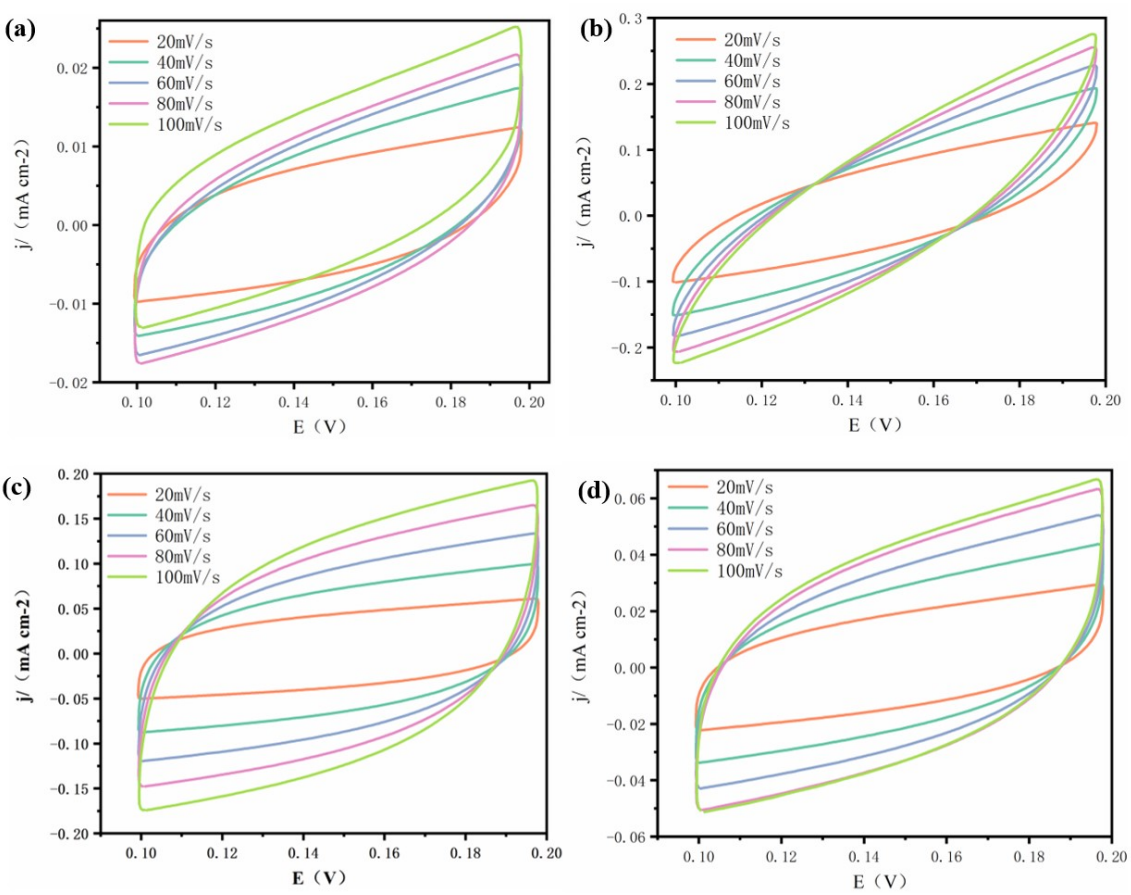

Figure S15. CV curves of (a)PBI-OP, (b) Ni_3P@Ni/CNP-L, (c) Ni_3P@Ni/CNP-M, and (d) Ni_3P@Ni/CNP-H.

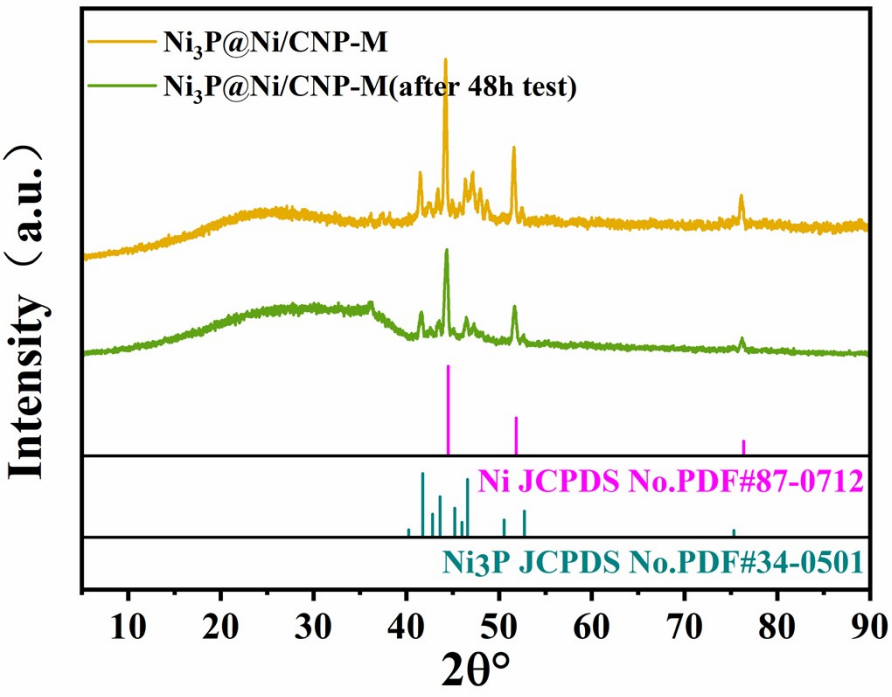

Figure S16. XRD pattern of Ni_3P@Ni/CNP-M after 48h test.

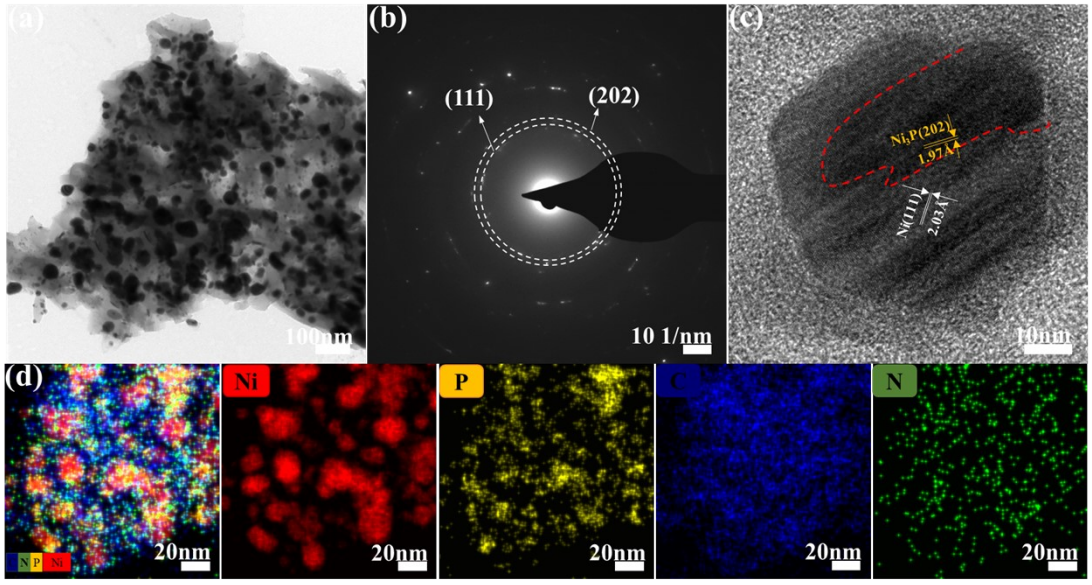

Figure S17. TEM of Ni_3P@Ni/CNP-M after 48h test.

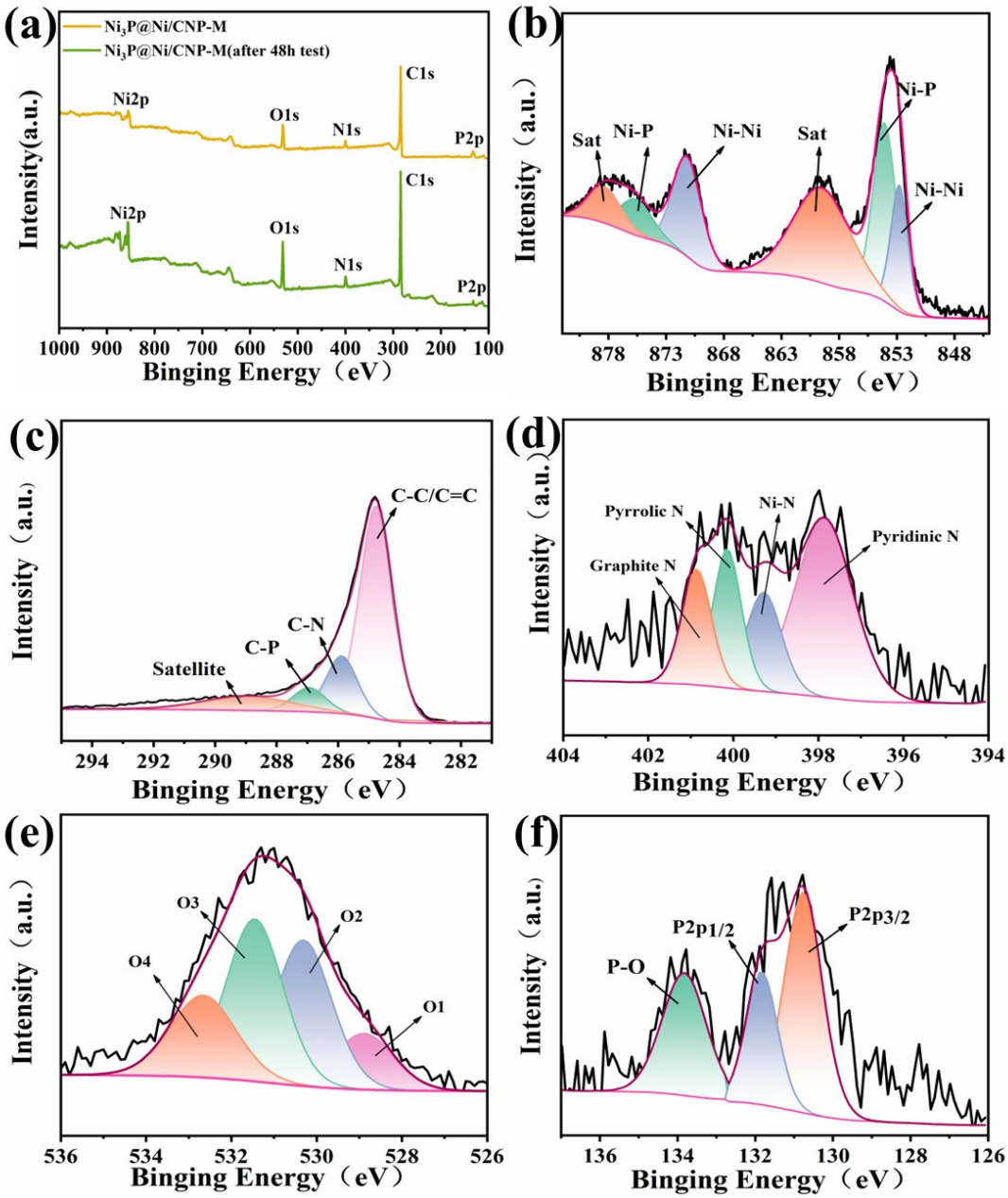

Figure S18. (a) XPS survey, (b) Ni2p, (c) C1s, (d) N1s, (e) O1s, and (f) P2p spectrums of Ni_3P@Ni/CNP-M after 48h test.

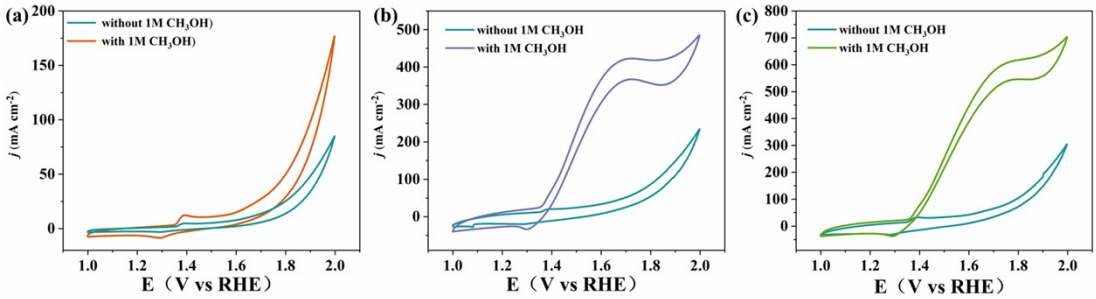

Figure S19. CV curves in 1M KOH before and after addition of 1 M CH_3OH of (a) PBI-OP, (b)Ni_3P@Ni/CNP-L and (c)Ni_3P@Ni/CNP-H.

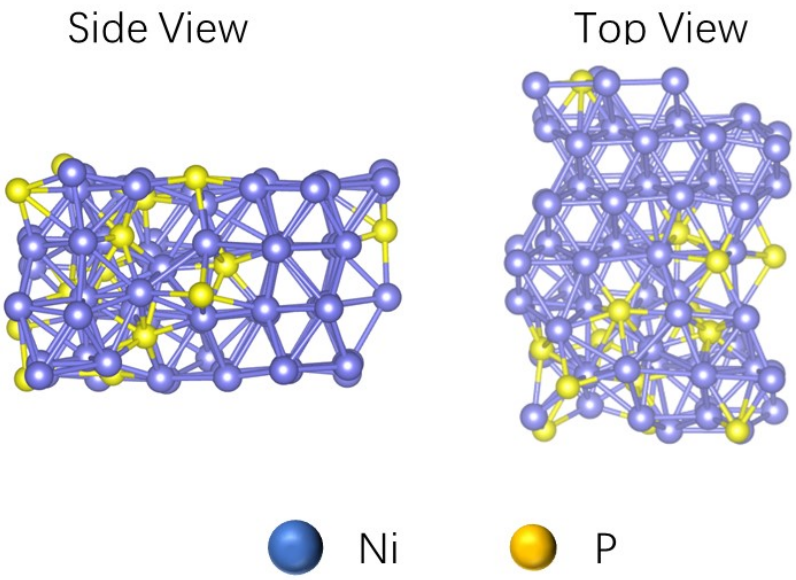

Figure S20.The optimized structure of Ni_3P@Ni, side view(left); top view(right). (lattice parameters a = 9.44 Å, b = 12.66 Å, c = 27.30 Å, α = 90°, β= 90°, γ= 90°).

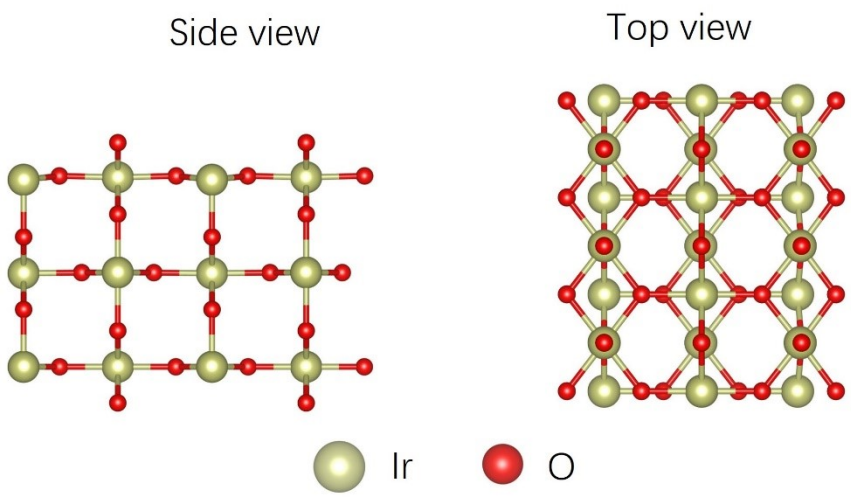

Figure S21. The optimized structure of IrO_2, side view(left); top view(right). (Lattice parameters a = 9.56 Å, b = 12.82 Å, c = 23.87 Å, α = 90°, β= 90°, γ= 90°).

Table S1. The surface area, total pore volume and pore size of PBI-OP, Ni_3P@Ni/CNP-L, Ni_3P@Ni/CNP-M, and Ni_3P@Ni/CNP-H.

Electrocatalyst	BET surface area ($m^2\ g^{-1}$)	Pore volume ($cm^3\ g^{-1}$)	Pore size (nm)
PBI-OP	12.03	0.023	7.60
Ni_3P@Ni/CNP-L	345.60	0.16	1.91
Ni_3P@Ni/CNP-M	**374.01**	**0.18**	**1.83**
Ni_3P@Ni/CNP-H	370.29	0.18	1.93

Table S2 Elemental and ICP-OES analyses of Ni_3P@Ni/CNP sample.

sample	elemental analysis（%）			ICP-OES analysis（%）	
	C	N	O	Ni	P
Ni_3P@Ni/CNP-L	41.06	1.16	3.53	47.82	6.33
Ni_3P@Ni/CNP-M	40.20	1.35	3.70	48.28	6.31
Ni_3P@Ni/CNP-H	40.31	2.07	3.45	48.03	6.09

Table S3. The XPS peak separation ratio of N1s for Ni_3P@Ni/CNP-L,Ni_3P@Ni/CNP-M and Ni_3P@Ni/CNP-H.

Electrocatalyst	Pyridinic N	Ni-N	Pyrrolic N	Graphite N
Ni_3P@Ni/CNP -L	40.15%	21.76%	19.5%	12.05%
Ni_3P@Ni/CNP -M	**43.1%**	**28.31%**	**11.45%**	**17.14%**
Ni_3P@Ni/CNP -H	32.81%	27.33%	23.19%	14.9%

Table S4. Comparison of electrocatalytic OER activities of Ni_3P@Ni/C-M with similar state-of-the-art OER catalysts.

	Electrolyte	j (mA cm^{-2})	η (mV)	Tafel slope (mV dec^{-1})	Ref.
Ni/Ni_2P@N-CNF	1.0 M KOH	10	285	52.2	**[22]**
N-Ni_3P-Ni/N-CNTs/NF	1.0 M KOH	10	270	98.59	**[23]**
Ni_3P/MnOOH	1.0 M KOH	10	300	79.8	**[25]**
Ni_2P/Co-NF	1.0 M KOH	10	316	81	**[27]**
NiFeP	1.0 M KOH	10	277	-	**[55]**
Ni/Ni_3C	1.0 M KOH	10	350	57.6	**[56]**
Ni_2P/$NiCo_2O_4$	1.0 M KOH	10	250	58	**[57]**
Ni_2P/NPCM NCs	1.0 M KOH	10	255	57	**[58]**
Ni_5P_4 NSs	1.0 M KOH	10	290	40	**[59]**
CNT@NiCoP/C	1.0 M KOH	10	297	57.35	**[60]**
Co_2P/Ni_2P@NF	1.0 M KOH	10	310	69.9	**[61]**
Fe_2P/Ni_2P HS/NF	1.0 M KOH	10	182	56	**[62]**
Fe-CoNiP	1.0 M KOH	10	280	99.1	**[63]**
NiFeP@CNT	1.0 M KOH	10	254	36.1	**[64]**
NiFeP@GNS	1.0 M KOH	10	211	43	**[65]**
NFP@NG	1.0 M KOH	10	295	57.7	**[66]**
NiP_2@FeP@CNT	1.0 M KOH	10	261	44	**[67]**
FeP/Ni_2P@CNT	1.0 M KOH	10	240	69.95	**[68]**
NiMn-P	1.0 M KOH	10	190	38	**[69]**
Ni_3P@Ni/C-M	**1.0 M KOH**	**10**	**239**	**52**	**This work**

Table S5 Elemental and ICP-OES analyses of Ni3P@Ni/CNP-M before and after 48h test.

sample	elemental analysis（%）			ICP-OES analysis（%）	
	C	N	O	Ni	P
Ni_3P@Ni/CNP-M	40.20	1.35	3.70	48.28	6.31
Ni_3P@Ni/CNP-M（after 48h test）	40.09	1.78	2.74	48.32	6.24

Table S6. EIS fitting parameters to the equivalent electric circuit for the OER.

	Ni_3P@Ni/CNP-L	Ni_3P@Ni/CNP-M	Ni_3P@Ni/CNP-H
Rs（Ω·cm²）	2.348	1.098	2.379
CPE（Ω·cm²）	3.1589E-5	2.7989E-5	2.8631E-5
Rct（Ω·cm²）	10.92	5.367	9.544